Antiviral Research 216 (2023) 105664

Contents lists available at ScienceDirect

Antiviral Research

journal homepage: www.elsevier.com/locate/antiviral

Inhibiting immunoregulatory amidase NAAA blocks ZIKV maturation in Human Neural Stem Cells

Michele Lai [a,b,*,1], Veronica La Rocca [a,c,1], Elena Iacono [a,d,1], Carolina Filipponi [a], Alessandro De Carli [a,d], Domenico Favaro [a], Rossella Fonnesu [a], Fabio Filippini [a], Pietro Giorgio Spezia [a], Rachele Amato [a,c], Elisa Catelli [a], Baggiani Matteo [e], Giulia Lottini [a,d], Marco Onorati [f], Nicola Clementi [g], Giulia Freer [a], Daniele Piomelli [h,1], Mauro Pistello [a,i,1]

[a] Retrovirus Center, Department of Translational Research and New Technologies in Medicine and Surgery, University of Pisa, Pisa, Italy
[b] Centre for Instrumentation Sharing, University of Pisa (CISUP), Italy
[c] Institute of Life Sciences, Sant'Anna School of Advanced Studies, Pisa, Italy
[d] Department of Medical Biotechnologies, University of Siena, Siena, 53100, Italy
[e] IRCCS Fondazione Stella Maris, Calambrone, Italy
[f] Unit of Cell and Developmental Biology, Department of Biology, University of Pisa, Pisa, 56127, Italy
[g] Laboratory of Medical Microbiology and Virology, Vita-Salute San Raffaele University, Milan, 20100, Italy
[h] Department of Anatomy and Neurobiology, University of California, Irvine, CA, 92697-4625, United States
[i] Virology Unit, Pisa University Hospital, Pisa, Italy

ARTICLE INFO

Keywords:
PEA
NAAA
Inflammation
Antiviral drugs
ZIKV
PPAR-α
ss(+)RNA viruses

ABSTRACT

Recent evidence suggests that lipids play a crucial role in viral infections beyond their traditional functions of supplying envelope and energy, and creating protected niches for viral replication. In the case of Zika virus (ZIKV), it alters host lipids by enhancing lipogenesis and suppressing β-oxidation to generate viral factories at the endoplasmic reticulum (ER) interface. This discovery prompted us to hypothesize that interference with lipogenesis could serve as a dual antiviral and anti-inflammatory strategy to combat the replication of positive sense single-stranded RNA (ssRNA+) viruses.

To test this hypothesis, we examined the impact of inhibiting N-Acylethanolamine acid amidase (NAAA) on ZIKV-infected human Neural Stem Cells. NAAA is responsible for the hydrolysis of palmitoylethanolamide (PEA) in lysosomes and endolysosomes. Inhibition of NAAA results in PEA accumulation, which activates peroxisome proliferator-activated receptor-α (PPAR-α), directing β-oxidation and preventing inflammation.

Our findings indicate that inhibiting NAAA through gene-editing or drugs moderately reduces ZIKV replication by approximately one $\log_{10}$ in Human Neural Stem Cells, while also releasing immature virions that have lost their infectivity. This inhibition impairs furin-mediated prM cleavage, ultimately blocking ZIKV maturation. In summary, our study highlights NAAA as a host target for ZIKV infection.

1. Introduction

Zika virus (ZIKV) is a positive-sense single-stranded RNA (ssRNA+) flavivirus that is transmitted by Aedes mosquitoes. Upon entering the cytoplasm, the naked RNA molecule of ZIKV is immediately translated into a polyprotein, and for Flaviviruses, this polyprotein is inserted cotranslationally in the endoplasmic reticulum (ER) and finally cleaved into three structural proteins (C, prM, and E) and seven nonstructural proteins (NS1, NS2A, NS2B, NS3, NS4A, NS4B, and NS5).

ZIKV has gained attention due to its ability to cross the placental barrier and cause several brain malformations in the fetus, including microcephaly (de Silva et al., 2018), during the ZIKV epidemics in Brazil (Butler, 2016; Heymann et al., 2016). ZIKV preferentially infects neural stem (NS) cells (Lottini et al., 2022) and there are currently no approved

* Corresponding author. Centro Retrovirus, Dipartimento di Ricerca Traslazionale e delle Nuove Tecnologie in Medicina e Chirurgia, Università di Pisa, SS 12 Abetone e Brennero, 2, Pisa, I-56127, Italy.
E-mail address: michele.lai@unipi.it (M. Lai).
[1] Authors provided equal contribution.

https://doi.org/10.1016/j.antiviral.2023.105664
Received 20 March 2023; Received in revised form 1 July 2023; Accepted 4 July 2023
Available online 4 July 2023

specific antiviral drugs for the treatment of ZIKV infection. However, various drugs are being tested in many studies that target different steps of the replication cycle. In this work, we hypothesize that blocking defined viral-induced inflammatory pathways might interfere with viral replication and/or maturation itself.

ZIKV boosts lipogenesis in infected cells to increase its replicative ability, thereby enhancing the production of pro-inflammatory lipid mediators, such as eicosanoids. Among them, arachidonic acid is released from phospholipids by various phospholipases (PLAs), including adipose triglyceride lipase and cytosolic PLA-A2α (cPLA2α) (Hammock et al., 2020; Adler et al., 2008). Free arachidonic acid can then be converted to inflammatory mediators, such as prostaglandins, prostacyclins, and thromboxane, by cyclooxygenases or to leukotrienes by lipoxygenases (Calder, 2020).

The enzyme cPLA2α, which is exploited by Flaviviridae and Coronaviridae, supports the genesis of viroplasm-like structures called replication organelles (RO), where encapsidation of ss(+)RNA occurs (Lai et al., 2022). This is probably why viruses belonging to the Flavivirus genus, such as Dengue virus and West Nile virus, upregulate cPLA2 (9, 10). It is plausible that viral infection by Flaviviridae turns on inflammation and lipogenesis at the same time, and thus, inhibition of lipogenesis may be hypothesized to reduce viral replication due to derangement of viroplasm-like structures(Dias et al., 2020). Several lipids are involved in blocking inflammation to enhance healing once viral infection is eradicated. These lipids include lipoxins, resolvins, and the N-acylethanolamines (NAEs), such as arachidonoylethanolamide (anandamide) and palmitoylethanolamide (PEA) (Keppel Hesselink et al., 2013). PEA is a well-recognized analgesic, anti-inflammatory, and neuroprotective mediator that exerts its anti-inflammatory action through activation of peroxisome proliferator-activated receptor-α (PPAR-α) (Taylor, 2013). PPAR-α drives PPAR response element gene transcription that spans from glucose and lipid metabolism to modulation of inflammation. Indeed, PPAR-α also interferes with the activity of proinflammatory transcription factors, including signal transducer and activator of transcription (STAT), as well as nuclear factor- κB (NF- κB) (Bougarne et al., 2018).

N-Acylethanolamine acid amidase (NAAA) is an N-terminal cysteine hydrolase that is present in the lysosomal compartment, Golgi cargoes and late endosomes of innate and adaptive immune cells and neuronal cells(Piomelli et al., 2020), where it catalyzes the hydrolytic cleavage of PEA, lowering its levels.

Taking into account the analgesic and anti-inflammatory properties of PEA, several NAAA inhibitors have been developed as anti-inflammatory drugs in the past decade(Migliore et al., 2016). These compounds have been found to have beneficial effects in various rodent models of human diseases, including inflammation(Gorelik et al., 2018), neuropathic pain (Sasso et al., 2013), chronic pain (Sasso et al., 2013), and lung inflammation (Wu et al., 2019). However, their role in viral infections is not well understood. NAAA inhibitors are believed to activate a cascade of biochemical events triggered by PPAR-α activation that alter lipid metabolism in a direction opposite to flaviviral infection. PPAR-α activation disrupts fatty acid droplets through β-oxidation in mitochondria and peroxisomes, while simultaneously stimulating ω-oxidation in microsomes(Yu et al., 2003).

In this study, we first investigated the relationship between ZIKV infection and NAAA expression. Next, we generated NAAA knockout cells and demonstrated that they are less susceptible to ZIKV replication. We then evaluated the potential of NAAA inhibitors as antivirals on neuronal stem cells. Finally, we show that NAAA inhibition slows down viral replication and, most importantly, inhibits viral maturation while simultaneously reducing inflammation.

2. Results

2.1. Interplay between NAAA expression and ZIKV replication

Viruses often modulate the expression of cellular components they require for replication (Zhang et al., 2016). We therefore hypothesized that NAAA levels may be elevated during ZIKV infection if NAAA played a role in viral replication. To test this hypothesis, we measured NAAA mRNA before and after ZIKV infection in A549 and Huh-7 cells, two well-established cellular models for ZIKV studies. As shown in Fig. 1a, cells were infected with ZIKV at 1 multiplicity of infection (MOI) for 1 h, and total RNA was collected from cell lysates at 24 and 48h post-infection (Fig. 1a). As a control, cells were transfected with polyI:C, a synthetic double-stranded RNA that mimics viral intermediate RNA molecules and activates the intrinsic cellular response (Yoneyama and Fujita, 2009). We found that both A549 and Huh-7 cells increased NAAA expression by ~2- and 3-fold, respectively, at 48h, whereas little difference was found at 24h (Fig. 1b). No difference was detected in polyI:C-transfected cells, indicating that the effect is ZIKV-specific and independent of TLR-3 activation, the PAMP receptor for viral dsRNA. To confirm NAAA up-regulation at the protein level, we probed ZIKV-infected A549 cells with both anti-NAAA and anti-ZIKV antibodies by high-content confocal immunofluorescence. Increased NAAA protein content was detected in ZIKV-infected cells, confirming that ZIKV infection causes a statistically significant increase in NAAA expression (Fig. 1c–e).

NAAA is modified in the Golgi apparatus by the addition of a mannose-6-phosphate recognition marker (M6P), which is critical for its trafficking into the lysosome (Čaval et al., 2019). ZIKV forms a toroidal-shaped structure, named viroplasm, in infected cells, to which microtubules, ER, and the Golgi apparatus closely associate (Caldas et al., 2020). We hypothesized that NAAA might mis-localize in viral replication organelles (ROs) during ZIKV infection, since NAAA is overexpressed during ZIKV infection and might be required for ZIKV replication. To test this hypothesis, we used high-content confocal microscopy to analyze the co-localization among ZIKV Capsid protein, NAAA, and trans-Golgi cargoes. To overcome the lack of suitable antibodies to simultaneously detect NAAA, ZIKV C and Golgin-97 vesicles, we separately determined co-localization of ZIKV and NAAA, ZIKV and Golgin-97 and NAAA and Golgin-97 as follows: first, we infected A549 cells with ZIKV, fixed them 48h after infection, and performed immunostaining for ZIKV capsid (C) protein and NAAA. The analysis showed that ZIKV C protein co-localizes with NAAA in ~80% of ZIKV virosomes marked in orange (Fig. 2a and b). We then probed cells treated the same way for Golgin-97, a marker of Golgi cargoes directed to the secretory pathway, and ZIKV. We found that ZIKV C protein co-localizes with Golgi trafficking vesicles in ~45% of ZIKV-C+ virosomes (Fig. 2c and d). Then, we repeated the experiment to confirm the presence of NAAA in Golgin-97+ vesicles and confirmed co-localization of NAAA with Golgin-97 in ~60% of vesicles analyzed in both infected and uninfected cells (Fig. 2e and f). Finally, we infected A549 cells and stained for ZIKV C protein NAAA and GOLGIN-97, then we 3D reconstructed their interactions. As shown in Fig. 2g, ZIKV infection reshapes ER and Golgi to form virosomes, in which NAAA clearly accumulates. In summary, NAAA is overexpressed and hijacked by ZIKV to the same Golgi-vesicles during infection and can be found in virosomes.

2.2. Ablation of NAAA interferes with ZIKV infection

To gain additional insight into the requirement of NAAA in ZIKV infection, we used CRISPR/Cas9 genome editing to generate $NAAA^{-/-}$ A549 cell lines, bearing frameshift mutations in both NAAA alleles. Production of $NAAA^{-/-}$ cell clones is described in Supplementary Information. To evaluate the effect of NAAA ablation on ZIKV replication, we infected A549 $NAAA^{-/-}$ clones with ZIKV at 1 MOI. In agreement with the previous results, plaque yield assays performed by infecting

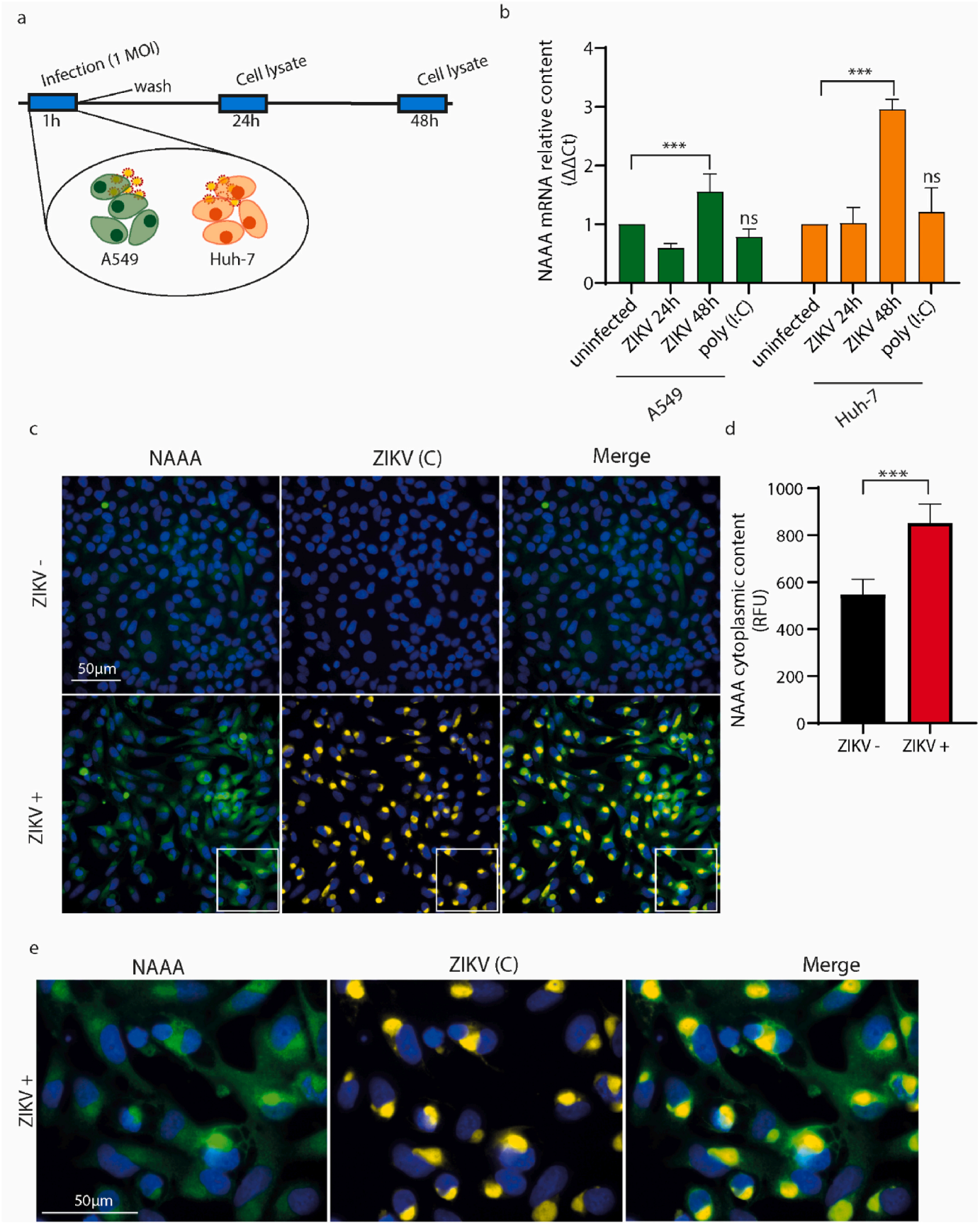

(caption on next page)

Fig. 1. NAAA expression increases after ZIKV infection. a. Schematic illustration of the experimental workflow. Briefly, A549 and Huh-7 cells were infected with 1 MOI of ZIKV and, 24 and 48h later, NAAA expression levels were measured in cell lysates. **b.** NAAA mRNA content, measured by qRT-PCR, in ZIKV infected lysates at 24 and 48h after infection. PolyI:C was used as control and transfected into cells at the same time as infection. Data are expressed as mean ± SD, N = 3, normalized with β-actin, and analyzed by One-way Anova (***$p < 0.001$, **$p < 0.01$, $\alpha = 0.05$). **c.** Immunofluorescence staining performed by high-content confocal microscopy of A549 cells infected or not with 1 MOI of ZIKV, 48h post-infection. Nuclei were stained with DAPI (blue), ZIKV Capsid(yellow), and NAAA (green). **d.** Statistical analysis of high content screening shown in c. Data are expressed as mean RFU ± SD, N = 3 and analyzed by One-way Anova (**$p < 0.01$, $\alpha = 0.05$). **e.** Representative images of immunofluorescence staining showed in c.

NAAA $^{-/-}$ as cell substrates with ZIKV revealed that complete NAAA ablation decreased ZIKV PFUs by 1 $\log_{10}$, while the heterozygous A549 clone NAAA $^{\pm}$ decreased ZIKV replication to a lower extent (5-fold reduction) (Fig. 3b). To confirm that ZIKV replication was reduced in the absence of NAAA, we performed a Western Blot analysis that showed decreased intracellular ZIKV envelope (E) protein content in the absence of NAAA, with a 2 $\log_{10}$ reduction in both A549 NAAA$^{-/-}$ and NAAA$^{+/-}$, compared to controls (Fig. 3c and d). NAAA is not present in early endosomes(Piomelli et al., 2020), therefore it could be argued that NAAA inhibition might influence egress of ZIKV (as illustrated in Fig. 3a). Thus, in the attempt to maximize the differences in ZIKV E content and exclude the possibility that NAAA$^{-/-}$ clones might enhance ZIKV E protein release, thereby reducing their E protein intracellular content, we also added Brefeldin-A, a drug that inhibits protein transport from the ER to the Golgi complex, blocking virion release (Fig. 3b and c). Again, addition of Brefeldin, and consequent retainment of protein E, highlighted the reduction in ZIKV E protein expression in the absence of NAAA. This also demonstrated that reduction in E content was not due to faster viral egress.

Finally, we measured the numbers of virions released by counting the number of ZIKV genomes in supernatants of each cell type by qRT-PCR at 3h, 24h, and 48h post-infection. To this aim, we added the 3h time point that allows to subtract the virions in the inoculum itself from the count of the virions produced. As shown in Fig. 3e, A549 NAAA$^{-/-}$ cells released a 5-fold lower number of particles in their supernatants, compared to WT counterparts.

On the whole, the results shown confirm that NAAA is required for ZIKV replication and its absence causes a decrease in viral production.

2.3. NAAA ablation creates a less permissive environment during ZIKV infection

To better elucidate how NAAA ablation affects host cells during ZIKV infection, we performed a transcriptomic analysis of A549 cells and their NAAA$^{-/-}$ cell clones, 24h after ZIKV infection. We identified 344 genes whose expression was significantly affected, with $\log_{10}$ fold change >1.5 in A549 NAAA$^{-/-}$ clones if compared to their WT counterparts. Among these, 32 genes involved in viral defenses, inflammation and ER-Golgi trafficking resulted to be the most affected, as shown in Fig. 4a, left panel. In particular, we show that NAAA$^{-/-}$ cells exhibit a 2-3-fold Log_{10} reduction in expression of RhoV and RhoB, described as key pro-viral mediators required by ZIKV during infection(Luu et al., 2021). We also found that ZIKV-Infected NAAA$^{-/-}$ cells exhibited one order of magnitude increase in expression of CX3CL1, a neuroprotective chemokine released by neurons after insults, if compared to their ZIKV-infected WT counterparts. Fig. 4a, right panel, summarizes the most striking differences between A549 and A549 NAAA-ablated clones in terms of activated pathways following ZIKV infection.

To better visualize the total changes in cellular pathways during ZIKV infection, we performed Gene Ontology (GO) enrichment analyses on cells. This allowed us to identify the specific biological processes, molecular functions, and cellular components that were significantly enriched or depleted in cells infected with ZIKV compared to uninfected cells. As shown in Fig. 4b, the analysis confirmed that the pathways that were affected the most by the absence of NAAA during ZIKV infection involved immune responses to stimuli and innate immunity. Interestingly, one of the most differentially expressed pathways was calcium-dependent exocytosis of neurotransmitters although with a low number of genes involved.

2.4. NAAA inhibitor ARN726 interferes with ZIKV replication

Given the negative effect of NAAA ablation on ZIKV replication, we then tested the antiviral activity of ARN726, a highly potent NAAA inhibitor, on A549 cells (Sasso et al., 2013). Toxicity assays revealed that ARN726 did not decrease cell viability when administered up to 20 μM (Supplementary Information 1). The drug was, therefore, administered at the concentration of 0.3, 1, 3, and 10 μM 15 min before ZIKV infection. Western blot analysis (Fig. 5a and b) shows dose-dependent ZIKV E protein reduction starting from 0.3 μM ARN726 treatment: at 3 μM, ARN726 reduced E expression by roughly 85%. To further confirm reduction in ZIKV replication, we measured the amount of ZIKV genomes in the supernatants of A549 cells treated with increasing concentrations of ARN726 by qRT-PCR (Fig. 5c). As expected, the analysis revealed a dose-dependent decrease of ZIKV genomes after ARN726 treatment, that reached its maximum inhibition after 3 μM at similar percentages of reduction observed in protein content. In agreement with the kinetics exhibited by NAAA −/− cells on ZIKV replication, which is visible starting from 48h post-infection, ARN726 as well did not have any effect at 24h but decreased the amount of ZIKV genomes significantly at 48h of treatment.

2.5. NAAA inhibitor ARN726 interferes with ZIKV replication in human neocortical neuroepithelial stem cells

Human neocortical neuroepithelial stem cells (NCX-NES) represent a major target of ZIKV infection for the fetus during pregnancy (Lottini et al., 2022). Thus, to probe whether NAAA inhibition might work as an antiviral strategy against ZIKV in human fetus derived NCX-NES, we repeated the same experiments shown in Figs. 1–5 on NCX-NES, as previously described (Lottini et al., 2022). We first measured NAAA mRNA levels in ZIKV-infected NCX-NES cells after 24h and observed a 3-fold increase in NAAA expression (Fig. 6a). These results agree with those reported above (Fig. 1), but the difference in NAAA mRNA levels appeared 24h earlier. Then, we evaluated the antiviral activity of NAAA inhibitor ARN726 against ZIKV also in NCX-NES cells, where no consequence on cell viability was found (Fig. 6b). The drug was administered 15 min prior to ZIKV infection at 3 and 30 μM; then viral RNA was measured on cell lysates and supernatants after 48h to better understand the level of replication (cell lysates) and virion release (supernatants). As shown in Fig. 6c and d, ZIKV viral RNA levels dropped by 40% and 75%, when ARN726 was administered at 3 and 30 μM, respectively. Then, we confirmed these results by using high-content confocal screening, as shown in Fig. 6e and f, using the amount of ZIKV infected cells (green) as a read out, counted out of total (number of nuclei). Again, as for A549, ARN726 decreased ZIKV-infected NCX-NES cell numbers by roughly 50% (Fig. 6f).

2.6. Assessing infectivity of virions produced by cells under NAAA inhibition

In the following sections, we performed experiments to shed light into the mechanisms whereby NAAA inhibition turned out to hinder viral infectivity. To start with, we performed viral yield reduction assays in the presence or not of GW6471, a potent inhibitor of the transcription factor PPAR-α, because the antiviral activity of NAAA inhibitor ARN726

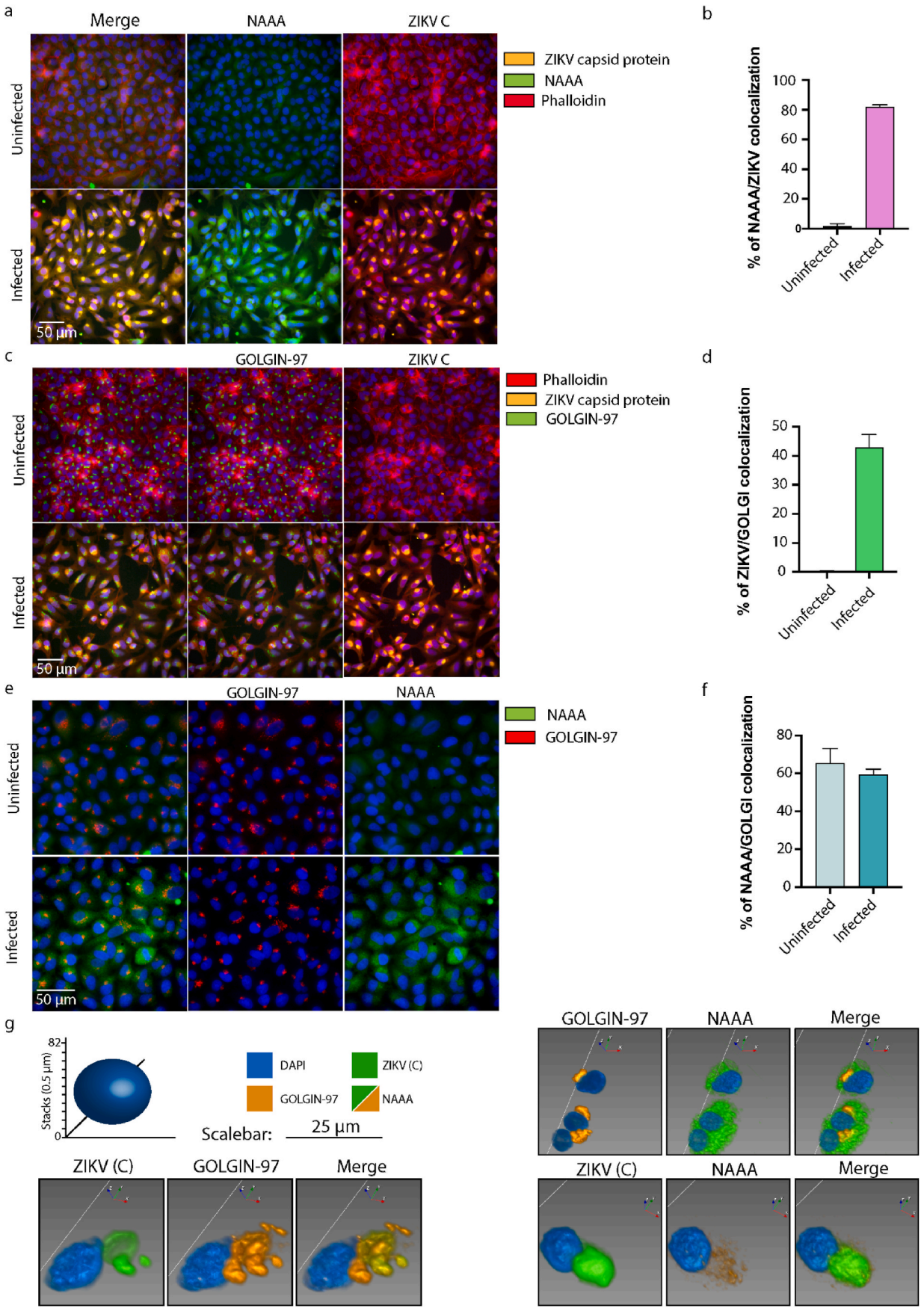

(caption on next page)

Fig. 2. NAAA co-localizes with ZIKV viroplasm. a. Representative images of A549 cells, infected or not with ZIKV at 1 MOI and stained for Phalloidin (DeepRed), ZIKV C protein (Orange) and NAAA (Green) 48h after infection. **b.** Statistical analysis performed on the high-content screening shown in a. Images (145 fields per sample) were analyzed with Harmony software to quantify co-localization of NAAA and ZIKV C protein in virosomes. **c.** Representative images of A549 cells, infected or not with ZIKV at 1 MOI and stained for Phalloidin (DeepRed), ZIKV C protein (Orange) and Golgin-97 (Green) 48h after infection. **d.** Statistical analysis performed on the high-content screening shown in c. Images (139 fields per sample) were analyzed with Harmony software to count the co-localization of Golgin-97 and ZIKV C protein in virosomes. **e.** Representative images of A549 cells, infected or not with ZIKV at 1 MOI and stained for NAAA (Green) and Golgin-97 (DeepRed) 48h after ZIKV infection. **f.** Statistical analysis performed on the High-content screening shown in e. Images (148 fields per sample) were analyzed with Harmony software to count the co-localization of Golgin-97 and NAAA in vesicles. Data are expressed as mean ± SD and analyzed with Student's T test, N = 3 (***$p < 0.001$; ns = not significant, $\alpha = 0.05$). **g.** 3D reconstruction of A549 cells infected with ZIKV and stained for NAAA, ZIKV C protein and Golgin-97. Images were taken by 82 stacks of 0.5 μm each.

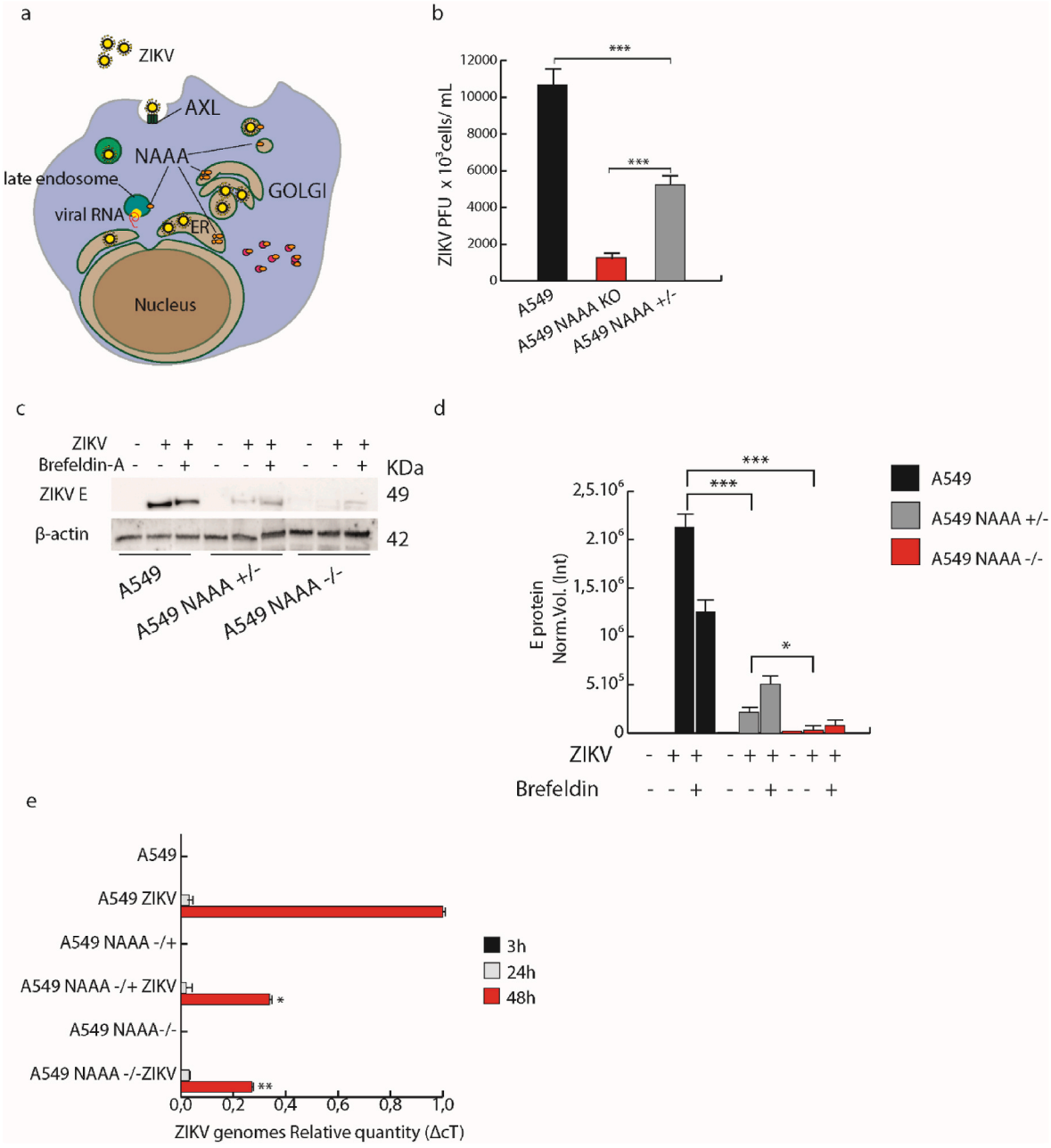

Fig. 3. NAAA ablation reduces ZIKV replication. a. Schematic illustration of ZIKV entry through the endocytic pathway and NAAA localization. **b.** Plaque assay performed on A549 and A549 NAAA$^{-/-}$ cells infected with 1 MOI of ZIKV. **c.** Western blot performed on A549, A549 NAAA $^{\pm}$ and A549 NAAA$^{-/-}$ using anti-ZIKV E and anti-Actin antibodies. **d.** Statistical analysis of the experiment shown in c. Data are expressed as mean ± SD, N = 4. **e.** qRT-PCR quantification of ZIKV viral genomes performed on supernatants of A549, A549 NAAA $^{\pm}$ and A549 NAAA$^{-/-}$, taken at 3h, 24h and 48h. Statistical analysis was performed using One-Way Anova ($p < 0.01$ *; $p < 0.001$ **; $p < 0.0001$ ***, $\alpha = 0.05$). Data are expressed as mean ± SD, N = 3.

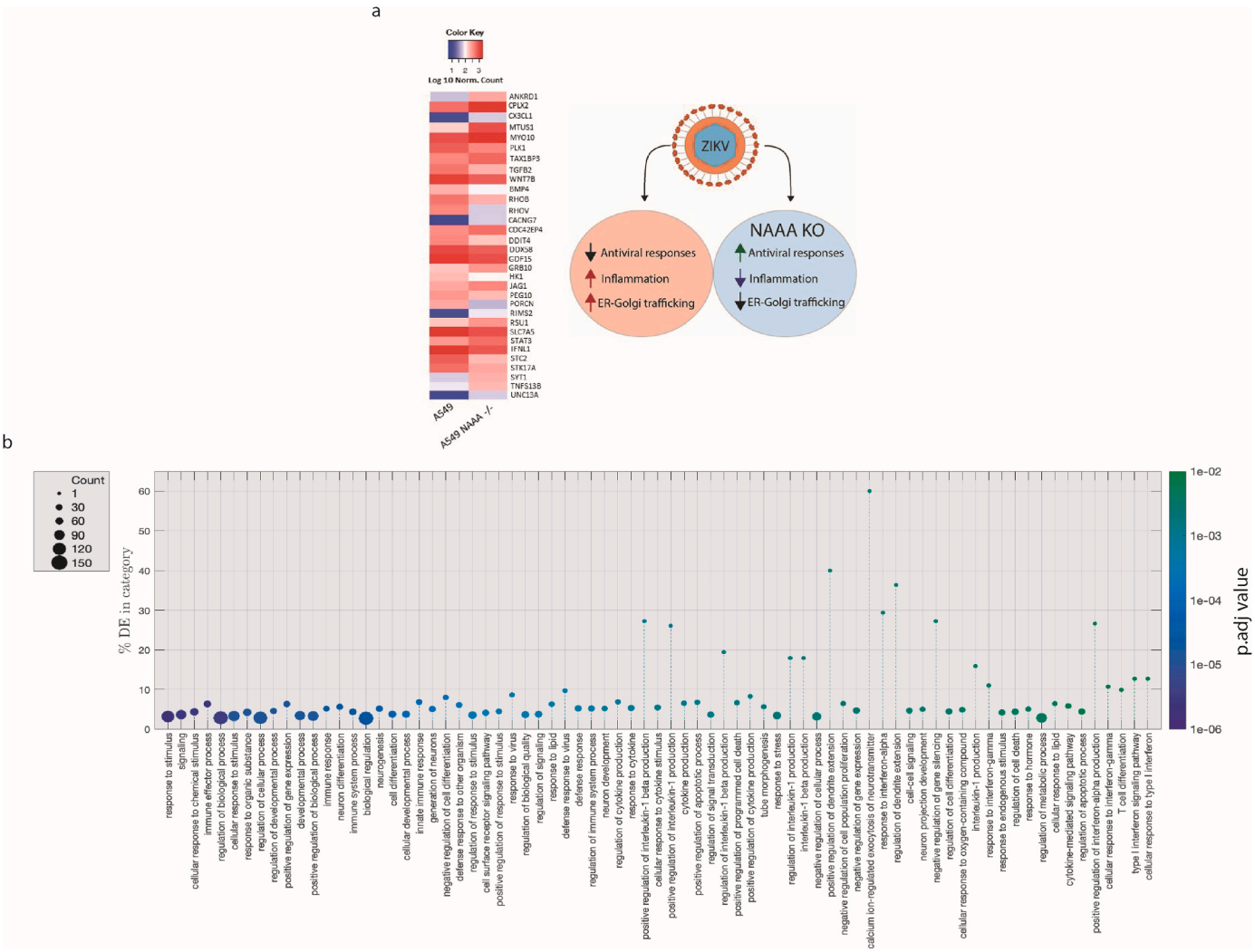

Fig. 4. Transcriptome analysis of differential expression between A549 NAAA$^{-/-}$ and WT cells after ZIKV infection. a. (left) Heatmap of Z scores on the most significantly affected genes. Colors indicate $\log_{10}$ normalized scale. (right) Schematic illustration of the most significantly affected expression pathways among the 32 genes represented in left panel. **b.** Bubble plot of genes significantly enriched in Gene Ontology assay in A549 or A549 NAAA−/− cells challenged with ZIKV. Left bar indicates adjusted p-value. Dot size indicates the number of genes differentially expressed in the same pathway as indicated in the box on the top left.

was initially thought to depend mostly on PPAR-α activation, which is mediated by the main substrate for NAAA, PEA. This assay allowed us to determine if PPAR-α was the only player mediating the antiviral activity of ARN726. Thus, we infected NCX-NES cells pretreated or not with ARN726, GW6471 (PPAR-α inhibitor) or both, as schematically illustrated in Fig. 7a. As shown in Fig. 7b, inhibiting PPAR-α has an opposite effect to NAAA inhibition and reverses it when given together with ARN726, increasing ZIKV viral genome release in supernatants by 7-fold, if compared to mock-treated (DMSO)/infected cells. This suggests that NAAA inhibitor exerts its effect on viral replication by activating PPAR-α. However, when the virions released by NCX-NES cells pretreated or not with ARN726 were used to further infect VERO E6 cells at the same genome units (Fig. 7c), virions generated by NCX-NES cells in the presence of ARN726, alone or together with GW6471, turned out to be less infectious that their counterparts generated by mock treated cells.

As shown in Fig. 7c, GW6471 alone did not affect infectivity of ZIKV particles, while the infectivity of virions released in the presence of ARN726 was ~95% lower, even when co-administered with GW6471. Thus, while the number of virions exiting cells is higher in ARN726/GW6471 treated NCX-NES cells (Fig. 7b grey bar), these virions are way less infectious than the once obtained with GW6471 alone. In summary, these results highlight that ZIKV replication impairment is mediated by PPAR-α activation, while ZIKV infectivity depends on an independent mechanism activated by the inhibition of NAAA.

2.7. NAAA inhibition protects NCX-NES against inflammation

The innate immune response during the acute phase of ZIKV infection is broadly inflammatory, as described by Kam et al. (2017). Indeed, a robust pro-inflammatory cytokine response occurs during acute ZIKV infection, with elevations of IL-18, TNF-α, IFN-γ, IL-8, IL-6, and other inflammatory mediators. Moreover, immune activation associated with increased CXCL10, IL-6, and IL-8 was also described in the amniotic fluid of ZIKV-positive pregnant women whose infants suffered from microcephaly (Ornelas et al., 2017). We probed if NAAA inhibitor ARN726 might contribute to quenching ZIKV-induced inflammation (Fig. 8a). Briefly we infected NCX-NES cells with ZIKV after pretreating with ARN726 (3 and 30 μM) for 15 min. Cell lysates were tested for expression of pro-inflammatory cytokines CXCL-10, IL-6, IL-8 by qRT-PCR (Fig. 8b), whereas cell supernatants were tested for IL-6 and IL-10 by ELISA assay (Fig. 8c). The administration of ARN726 reduced the transcription of CXCL-10, IL-6 and IL-8 in NCX-NES cells by at least two-fold after ZIKV infection. We also observed a dose-dependent

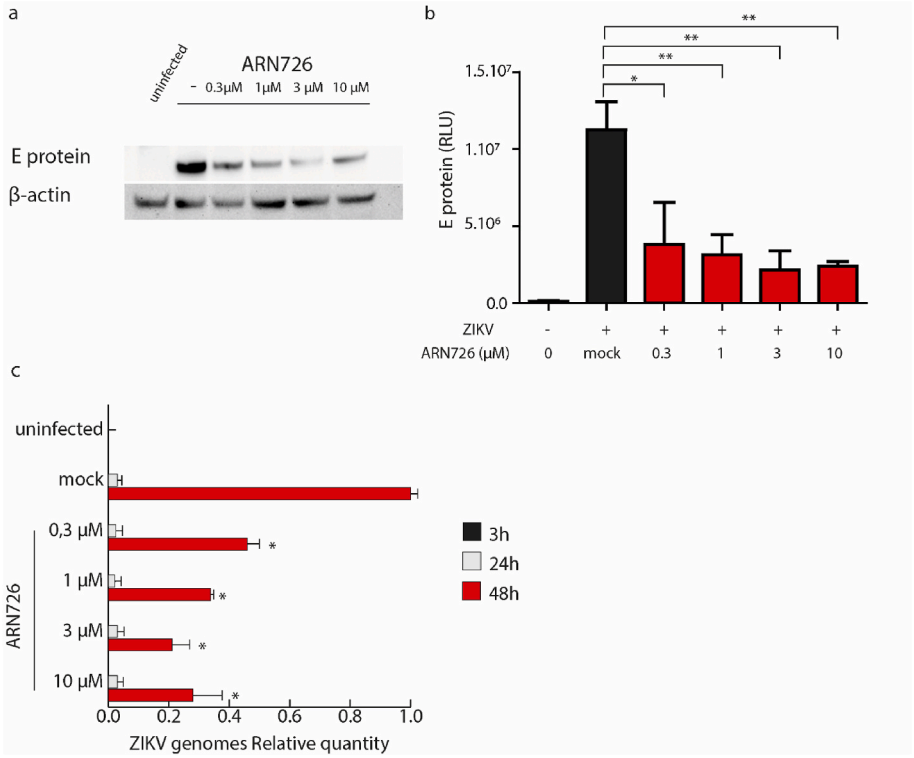

Fig. 5. NAAA inhibitor ARN726 decreases ZIKV replication. a-b. Western blot performed on lysates of A549 cells treated with increasing doses of ARN726 15 min before ZIKV infection, using anti-ZIKV E and anti-actin antibodies. Statistical analysis was performed using One-Way Anova ($p < 0.001$ **; $\alpha = 0.05$). Data are expressed as mean ± SD, N = 4. **c.** qRT-PCR quantification of ZIKV viral genomes performed on supernatants of A549 cells treated with increasing doses of ARN726 15 min before infection. Supernatants were taken at 3h, 24h and 48h post-infection. Statistical analysis was performed using One-Way Anova ($p < 0.01$; $\alpha = 0.05$). Data are expressed as mean ± SD, N = 5.

decrease in the release of IL-6 and IL-10 in NCX-NES cells treated with ARN726 if compared to untreated-infected counterparts (Fig. 8c). The anti-inflammatory activity was paralleled by an increase in PPAR-α expression, as determined by qRT-PCR on the same cell lysates. This is expected since it is known that, once activated by PEA, PPAR-α increases its expression by a positive feedback loop (Fig. 8d)(Mottillo et al., 2012). Also, PGC1-α, one of the main co-activators of PPAR-α, turned out to be over-expressed after NAAA inhibition (Fig. 8d). These results highlight that NAAA inhibitors quench inflammation, in addition to suppressing ZIKV infectivity.

2.8. NAAA inhibition hinders prM maturation

Because infectivity of virions released by ARN 726-treated cells was much lower than by their mock-treated counterparts at equal amounts of genomic units/cell (Fig. 7), we hypothesized that NAAA inhibition might interfere with virion maturation. Flaviviral particles are believed to mature by cleavage of prM precursor to M and pr proteins within the trans-Golgi network(Yu et al., 2008, 2009; Sirohi and Kuhn, 2017). Indeed, maturation relies on Furin, a host protease capable of cleaving ZIKV prM only at a precise acidic pH of ~5(29), while only in that pH range prM exposes its catalytic sites to furin(Cortese et al., 2019). Therefore, we determined the amount of precursor prM and mature M proteins present on the surface of virions released in the presence or absence of ARN726, as a measure for virion maturation, as previously done by Cortese et al. (2019). To this aim, we infected A549 cells, pre-treated or not with ARN726, with ZIKV at 1 MOI (Fig. 9a). Virions released were harvested 48h p.i and analyzed for M/prM (mature vs immature) content by Western blot. As shown in Fig. 9b and c, ARN726-treated A549 cells released immature virions, with a 75% reduction in M content. Similar results were obtained also on virions released by NCX-NES cells (Supplementary Information 2). This result is in agreement with the fact that treatment with ARN726 caused almost no release of infectious virions for VeroE6 cells, as reported in Fig. 7h and I.

A possibility might be that prM cleavage is hindered by increasing intra-vesicular pH, thus blocking the conformational change allowing access to viral surface protein (Yu et al., 2008). NAAA enzyme might contribute to maintaining acidic pH by degrading PEA into palmitic acid and ethanolamine in the vesicles where it is colocalized with ZIKV proteins (Fig. 2). Once NAAA is inhibited, palmitic acid is no longer released and PEA accumulates, ultimately increasing vesicular pH. To confirm this hypothesis, we probed the ability of ARN726 to affect vesicular pH by treating A549 cells with Lysosensor Blue/yellow dye. This molecule allows to determine the pH of vesicles precisely by calculating the ratio between blue fluorescence (less acidic) and yellow (more acidic) fluorescence intensity. To do so, we pre-treated A549 cells with ARN726 at increasing concentrations (0.03, 0.3, 3, and 30 μM), and using Chloroquine or untreated (DMSO) cells as basification control and background control, respectively. Then, cells were stained for membrane (CellMask 687), nuclei (DAPI) and Lysosensor Blue/Yellow. Then, cells were analyzed by high content confocal screening (Fig. 9d,g). Fig. 9d–f show that ARN726 increased vesicular pH to ~6, when administered above 0.3 μM, compared to pH ~4 of their DMSO-treated counterparts.

2.9. NAAA inhibition reduces Furin activity

To further confirm that impairment of Furin cleavage is the primary mechanism responsible for the observed anti-maturation effect during NAAA inhibition, we treated A549 cells with or without ARN726 for 24h. Then cells were incubated with BOC-RVRR-AMC, a synthetic fluorogenic substrate that is efficiently cleaved by furin leading to fluorescence emission (Fig. 10 a-b). As shown in Fig. 10c, ARN726 treatment reduced Furin activity by roughly 60%. If the anti-maturation activity of ARN726 depends on Furin reduced activity, viruses that do not rely on Furin for maturation should not be affected by treatment with ARN726. To test this hypothesis, we infected A549 cells with Vesicular Stomatitis Virus (VSV) and Coxsackievirus B5 (COXB5) at a 0.1 MOI (multiplicity of infection). Neither of these viruses relies on Furin for maturation.

VSV is a bullet-shaped negative-stranded RNA virus that possesses approximately 400 trimeric transmembrane spikes composed of a single

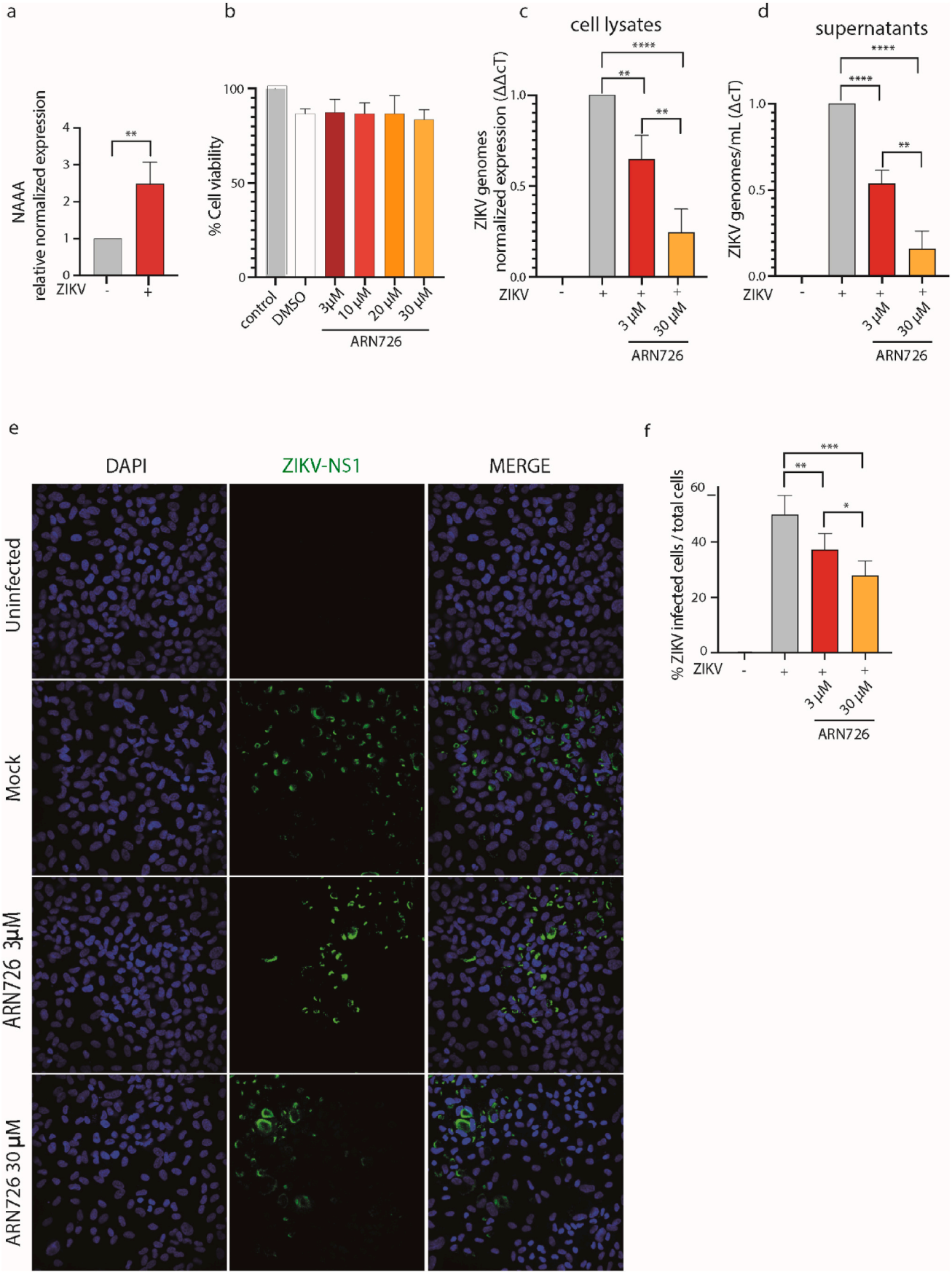

(caption on next page)

Fig. 6. NAAA inhibition hinders ZIKV maturation in NCX-NES cells. a. qRT-PCR quantification of NAAA mRNA relative content, performed on NCX-NES cells before and after 24h of ZIKV infection (0.5 MOI). **b.** WST-8 cell viability assay on NCX-NES cells, treated with increasing concentrations of ARN726. **c-d.** qRT-PCR quantification on ZIKV genomes performed on lysates (c) and supernatants (d) of NCX-NES cells treated or not with ARN726 at 3 and 30 μM. ZIKV genomes detected on lysates were normalized on β-actin content (ΔΔcT). **e.** High-content confocal screening performed 48h after NCX-NES cells infection with ZIKV (0.5 MOI). Briefly, cells were pre-treated or not with 3 and 30 μM ARN726, then infected for 48 h and fixed and stained for ZIKV NS1 protein. Analysis by high-Content confocal microscopy was carried out with the following building blocks: Find Nuclei (Dapi)> find cytoplasm (Digital Phase Contrast) > find spots (ZIKV NS1) > select population (ZIKV + cells)> Calculate n° ZIKV + cells/total **f.** Statistical analysis performed on the High-Content Screening assay. Data are expressed as mean ± SD and analyzed with One-Way Anova (**p < 0,01; ***p < 0.001; α = 0.5.).

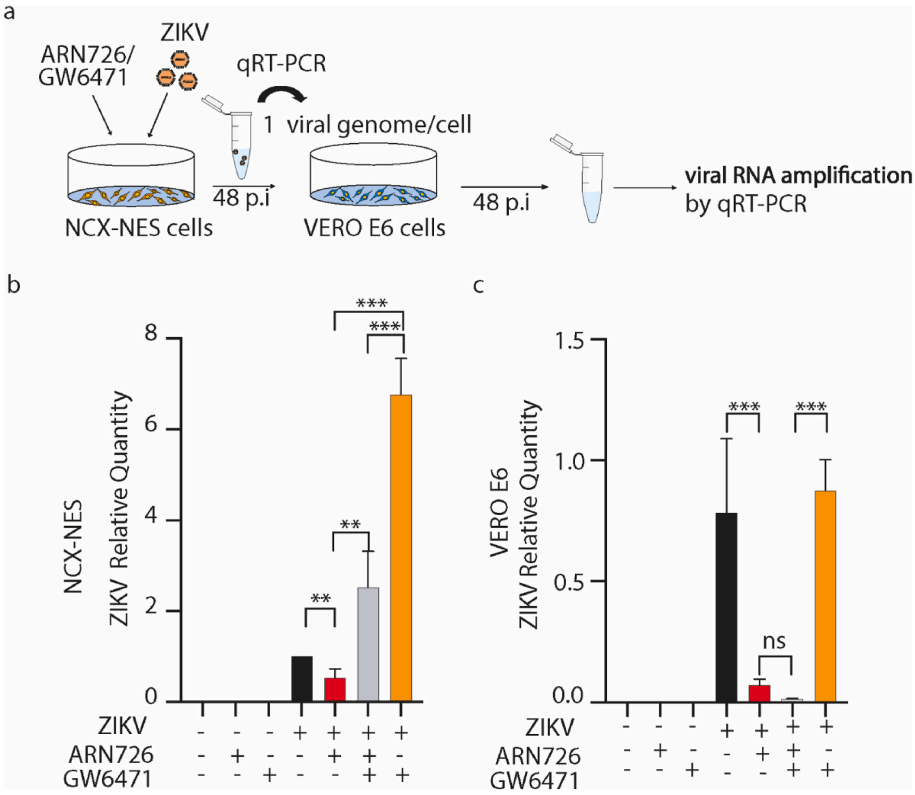

Fig. 7. NAAA inhibitor ARN726 decreases infectivity of ZIKV viral progeny in NCX-NES cells while PPAR-α inhibitor does not. a. Schematic workflow to assess infectivity of ZIKV released by NCX-NES cells in the presence of NAAA inhibitor ARN726 (30 μM) and/or PPAR-α inhibitor GW6471 (1 μM). Briefly, NCX-NES were pre-treated with one or both inhibitors and infected with ZIKV (MOI 1); supernatants were collected 48h later and titered for ZIKV genomes by qRT-PCR. Then, the same number of genomes were administered to VERO E6 cells, to evaluate infectivity. **b.** qRT-PCR quantification on ZIKV genomes performed on supernatants of NCX-NES cells treated with one or both inhibitors, collected 48h after infection. Data are expressed as mean ± SD and analyzed with One-Way Anova (**p < 0.01, ***p < 0.001 α = 0.5). **c.** Statistical analysis performed on qRT-PCR quantification of ZIKV genomes released by VERO E6 cells, infected with 1 ZIKV genome/cell released by NCX-NES cells, treated or not with ARN726 and GW6471. Data are expressed as mean ± SD and analyzed with One-Way Anova (ns = not significant, ***p < 0.001, α = 0.5).

viral glycoprotein G, as its envelope. This protein does not need specific pH to be activated by proteases (Da Poian et al., 2005)(Fig. 10a).

Similarly, COXB5 is a small non-enveloped RNA virus belonging to the Picornaviridae family. Its maturation process relies on self-cleavage activity of structural proteins (Basavappa et al., 1994), as depicted schematically in Fig. 10c.

We collected supernatants from ARN726-treated and untreated A549 cells. The viral genomes in the supernatants were quantified using qRT-PCR, and the resulting viral titers were used to infect VERO cells using 1 viral genome/cell. As depicted in Fig. 10b–d, no reduction in infectivity was observed for both viruses when using supernatants derived from untreated or treated cells. These results support the hypothesis that NAAA inhibition might cause intravesicular changes that affect prM processing and maturation.

3. Discussion

In the present work, we set out to test the antiviral activity of ARN726, an anti-inflammatory compound that acts by inhibiting NAAA, and ended up uncovering that, although inhibiting inflammation decreases ZIKV replication, the most significant effect of NAAA inhibition of ZIKV virion release is obtained by inhibiting maturation.

Our hypothesis that anti-inflammatory compounds might act as antiviral drugs while avoiding virally induced excessive inflammatory response relies on several converging nodes between inflammation and ssRNA + viral replication. Once ssRNA + viral infection starts, lipogenesis is enhanced, as a hallmark of replication and inflammation, to supply energy and lipids necessary for both processes (Martín-Acebes et al., 2016). It is therefore not surprising that β-oxidation, the main route of lipid dismantling, is suppressed by several viruses (Lai et al., 2022). Given these premises, we hypothesized that reversion of ZIKV-induced lipogenesis might interfere with replication organelle formation during flaviviral infections.

To probe the role of NAAA during ZIKV replication, we first assessed whether NAAA might be upregulated during ZIKV infection, as happens for many cellular factors required by viruses for their replication (Lai et al., 2022). We show here that NAAA is upregulated during infection and localizes in ZIKV viroplasms. The latter finding is interesting because NAAA normally localizes to endosomes/lysosomes, and therefore appears to be recruited by the virus specifically. Indeed, ZIKV reshapes ER and Golgi and partially fuses them together to create viroplasms (Caldas et al., 2020). Since NAAA reaches lysosomes through the Golgi apparatus, where the enzyme receives its M-6-P tag for lysosomal trafficking, NAAA might be recruited in the viroplasm itself and cause intravesicular changes during ZIKV egress.

Next, we generated four cell lines derived from A549 where NAAA was ablated by frame-shift mutations in the first exon of the *ASAHL* gene. These cells were infected with ZIKV and replication efficiency and virion infectivity were analyzed. We discovered that ZIKV replication decreases by ~1 $\log_{10}$ when NAAA is abolished.

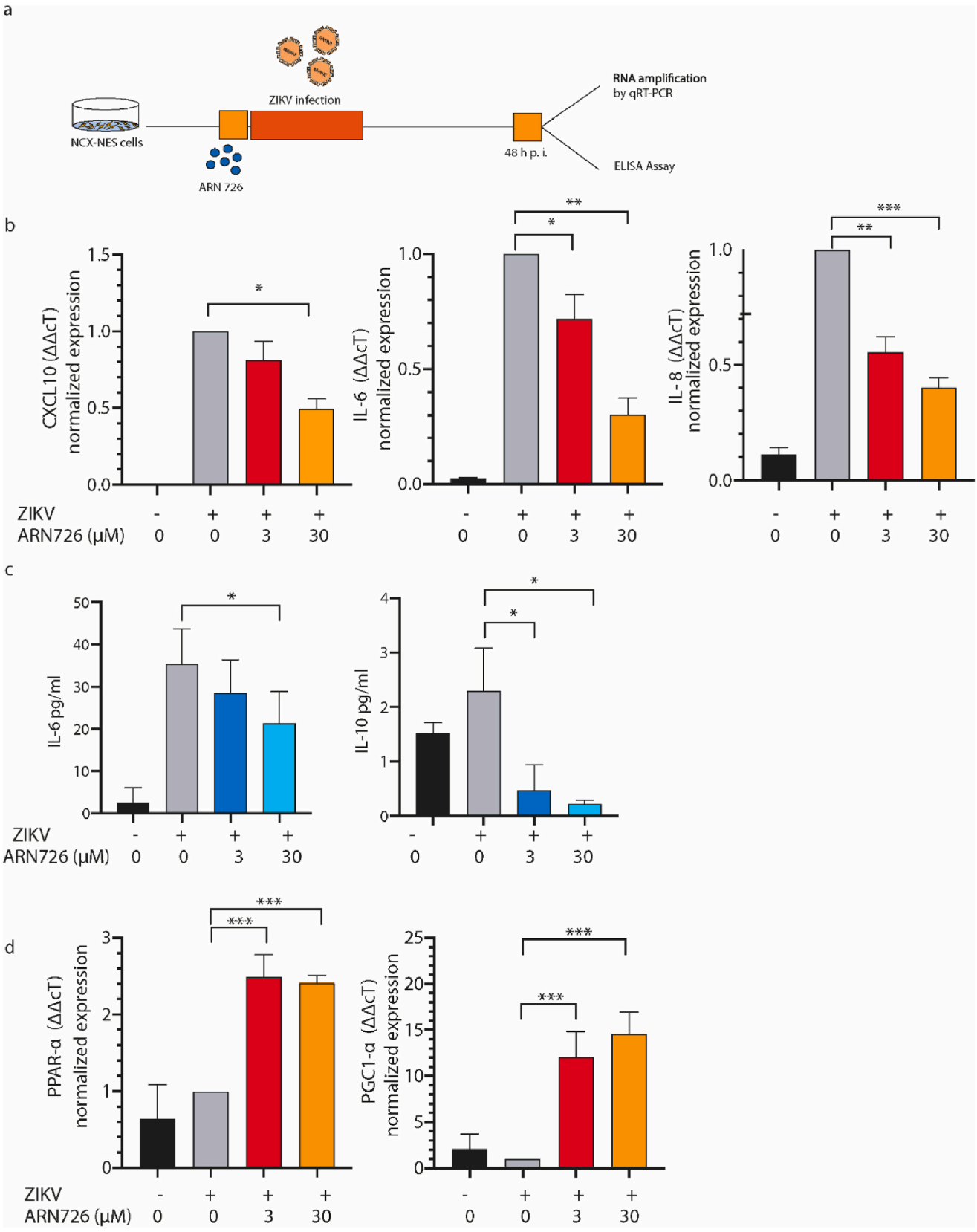

Fig. 8. NAAA inhibition quenches inflammation in NCX-NES cells. a. Schematic illustration of experiments presented in b,c,d. **b.** qRT-PCR quantification of CXCL10, IL-6 and IL-8 performed on NCX-NES cells infected or not with ZIKV (1 MOI) and treated or not with ARN726 (3 and 30 μM) before ZIKV infection. **c.** ELISA assay performed on supernatants collected from NCX-NES cells infected or not with ZIKV (1 MOI) and treated or not with ARN726 (3 and 30 μM). **d.** PPAR-α and PGC1-α mRNA relative content in NCX-NES cells infected or not with ZIKV (1 MOI) and treated or not with ARN726 (3 and 30 μM). Data are expressed as mean ± SD, N = 3 and analyzed with One-way Anova (*$p < 0.1$; **$p < 0.01$ ***$p < 0.001$, $\alpha = 0.05$).

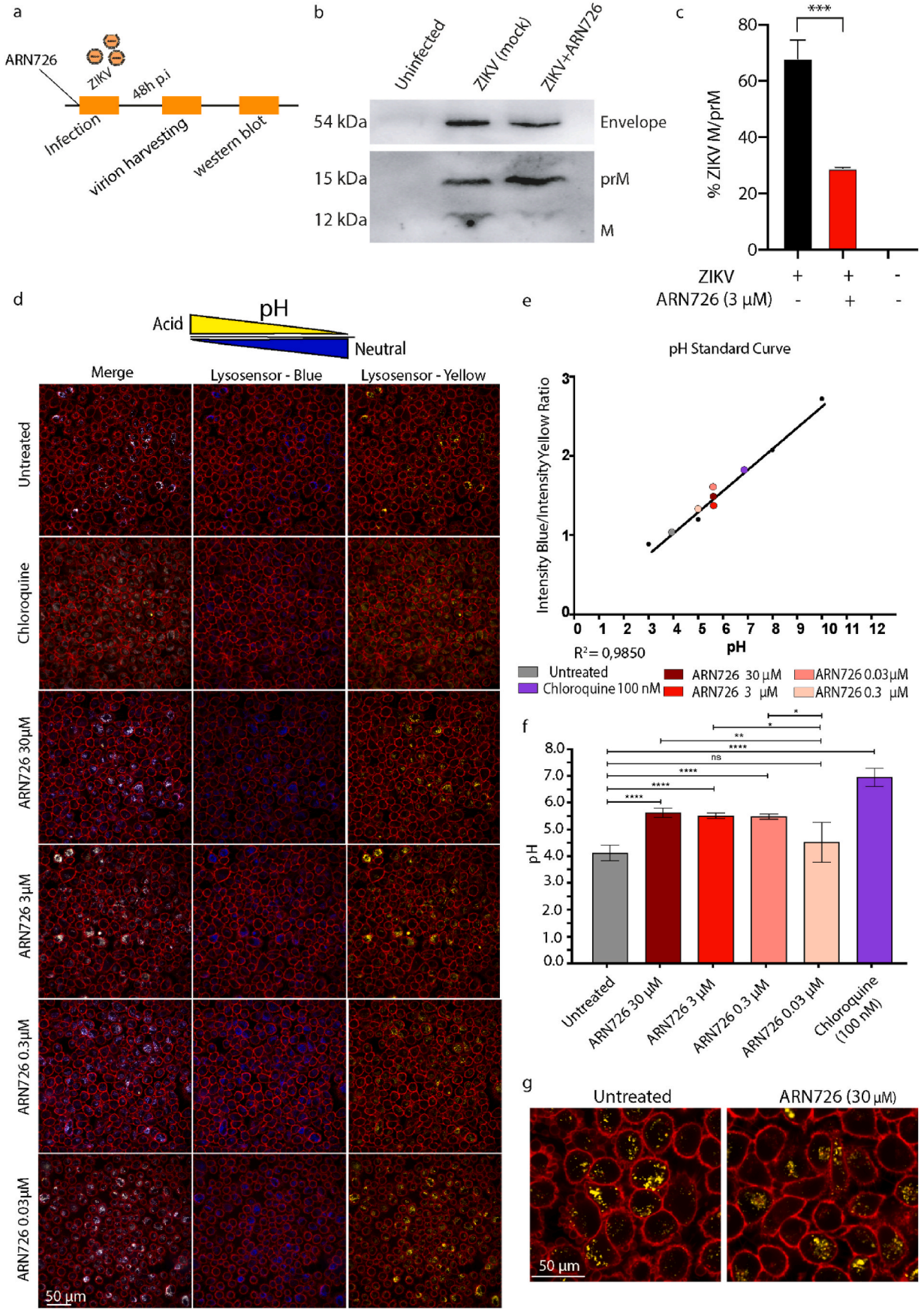

(caption on next page)

Fig. 9. ARN726 hinders virion maturation and increases vesicular pH.
a. Schematic workflow of virion extraction by ultracentrifugation. A549 cells, pre-treated or not with ARN726 at 0.03–30 μM, were infected with ZIKV at 1 MOI. Virions released were harvested 48h p.i and analyzed for M/prM (mature vs immature) content by Western blot. **b.** Western blot analysis of prM and M content performed on virions released in the presence or not of ARN726. ZIKV E protein was used to normalize prM/M ratio **c.** Statistical analysis performed on M/prM ratio. Data are expressed as mean ± SD and analyzed by Student's T test, N = 3 (***p < 0.001 α = 0,5) **d.** High content confocal screening performed on A549 cells treated or not with ARN726 (24h) and Cloroquine (100 nM) for 1h. Cells were then treated with Lysosensor, Blue/Yellow to stain intracellular acidic vesicles, and Cell Mask (deep red) to stain cell membranes. Cells were acquired using a 63 × water objective and then analyzed for blue/yellow intensity in every spot detected. **e.** Standard curve of A549 cells obtained by treating cells with Lysosensor blue/yellow, then exposing samples to buffers at different pH (Heymann et al., 2016; Lottini et al., 2022; Hammock et al., 2020; Adler et al., 2008; Calder, 2020; Lai et al., 2022; Merad and Martin, 2020; Wang et al., 2022; Dias et al., 2020; Keppel Hesselink et al., 2013) and acquired with the same parameters shown in d. **f.** Statistical analysis of pH variations among samples shown in d. Data are represented as mean ± SD and analyzed with One-Way Anova (*p < 0.1, **p < 0.01, ****p < 0.0001; α = 0,5). **g.** Representative images of A549 cells treated or not with ARN726 (30 μM) and live-stained with Lysotracker yellow/blue, taken from high-content screening shown in a. Cell membranes were stained with CellMask-Deep Red and acidic vesicles with Lysotracker Blue/Yellow.

We then tested the antiviral efficacy of NAAA inhibitor ARN736, a well-established anti-inflammatory drug used to treat neuropathic pain and inflammation (Piomelli et al., 2020). This compound is known to exert its anti-inflammatory activity by switching off lipogenesis and boosting β-oxidation (Piomelli et al., 2020). In our experiments, a strong antiviral effect was observed using human fetus-derived NCX-NES cells, primary targets of ZIKV. Once NAAA was blocked, ZIKV replication decreased and, consequently, also virion release dropped abruptly by ~5-fold. We assessed that the drop in ZIKV replication during NAAA inhibition is PPAR-α dependent, since the addition of PPAR-α inhibitors restore ZIKV replication in NAAA-inhibited cells. Surprisingly, we discovered that ZIKV virions released in the absence of NAAA activity lost ~98% of their infectivity, if compared to their counterparts released by untreated cells. At the same time, we also showed that lack of virion maturation did not depend on activation of PPAR-α-related pathways, highlighting a dual mechanism for ARN726 to inhibit ZIKV release. Indeed, co-administration of ARN726 (NAAA inhibitor) and GW6471 (PPAR-α inhibitor) resulted in the release of immature virions, while the administration of GW6471 alone actually boosted ZIKV replication without affecting maturation. Most notably, lack of infectivity depended on the release of immature virions where prM content, a hallmark of immature virus, in virions released by NAAA-inhibited A549 and NCX-NES cells resulted largely increased, suggesting defects in Furin cleavage of the viral protein (Sirohi and Kuhn, 2017). Prompted by these findings, we hypothesize that the reason behind the lack of virion maturation relies on impaired Furin optimal activity. Indeed, flavivirus maturation requires Furin(Stadler et al., 1997), a cellular protease located primarily in the trans-Golgi network (Molloy et al., 1994), capable of cutting flaviviral precursor membrane protein (prM) into mature M protein. Increasing vesicular pH from acidic to neutral impairs Furin access to prM cleavage site(Stadler et al., 1997), causing the release of immature virions, which are way less infectious (Stadler et al., 1997; Vaney et al., 2022). In line with our hypothesis, when we measured A549 vesicular pH after the administration of ARN726, we discovered that it shifted from ~4 to ~6, when NAAA is inhibited. Increased vesicular pH might be explained by the impaired cleavage of PEA. Indeed, when NAAA is active, it cleaves PEA in palmitic acid and ethanolamide, contributing to acidifying vesicles. Once NAAA is blocked, PEA accumulates and palmitic acid is no longer released, causing a raise of vesicular pH. At this pH, prM does not have the correct conformation for its cleavage by Furin; however, Furin itself does not seem to work as efficiently when NAAA is inhibited as shown in Fig. 10c. It's tempting to speculate that Ca2+ might be involved since several genes found to be differentially expressed in NAAA−/− cells infected with ZIKV were involved in Ca2+ homeostasis. Unsurprisingly, the replication of viruses like VSV and COXB5, who do not rely on Furin for their maturation, was not affected by ARN 726 treatment (Fig. 10).

Together, these results highlight for the first time that a well-recognized anti-inflammatory agent can be also used as an anti-flaviviral drug. While NAAA was never studied as an antiviral target until now, its substrate PEA has been used in several placebo-controlled double-blind clinical trials against SARS-CoV-2 and other respiratory viruses(Di Stadio et al., 2022). Promising results led to the clinical use of PEA under the brand name Impulsin in former Czechoslovakia (Keppel Hesselink et al., 2013). As PEA plays a fundamental role as an anti-inflammatory, lipid-modulating precursor, its activity is counteracted by NAAA, which is abundant not only in neuronal cells, but also in macrophages and immune cells (De Filippis et al., 2013), the very cells responsible for cytokine storm in severe COVID19. For this reason, while the antiviral activity of PEA might not be durable, NAAA inhibition might have a longer-lasting efficacy and more potent anti-inflammatory/antiviral activity, especially when administered in combination with PEA.

In summary, this work unveils NAAA as a critical host factor not only for ZIKV replication, but for Flaviviruses in general and for all those viruses that rely only on Furin for their maturation.

4. Materials and methods

4.1. Cell culture, transfection, and treatments

A549 and Huh-7 cells were purchased from American Type Culture Collection (Manassas, VA 20110, USA), and cultured at 37 °C in 5% CO2 in Dulbecco-Modified Eagle's Medium (DMEM) supplemented with 10% fetal bovine serum (FBS), 100 U/mL penicillin and 100 μg/mL streptomycin. Cells were seeded in 96-well plates and transfected 24h after with pMXs GFP-LC3-RFP (#117413, Addgene, MA) or with Polyinosinic–polycytidylic acid sodium salt, Poly (I:C) (0.5 ng/μL), using Lipofectamine LTX and PLUS reagent (Thermo Fisher Scientific, Waltham, MA 02451, USA) according to the manufacturer's instructions. Cells were tested for mycoplasma contamination as previously described (Lai et al., 2021a). Human NCX-NES cells were maintained in NES medium and split, when confluent, once every 5–7 days as previously described (Lottini et al., 2022).

4.2. CRISPR/Cas9 design and transfection

A549 cells were transfected with CRISPR/Cas9 RNP (IDT, Coralville, Iowa) by nucleoporation (NEON Electroporation System, Thermo Fisher, Massachusetts, USA) using the following parameters: 1200 V, 30 ms, 2 pulses using the sgRNA guide: AGTGGGTGCACGTGTTAATC. To isolate single-cell clones, cells were seeded in 96-well performing a single-cell limiting dilution protocol as previously described(Lai et al., 2021b, 2021c, 2021d). Edited clones were selected by sequencing analysis of PCR products, using the following primers: F 5′-GAGGCTGCAGATTGAGTGAC-3′, R 5′- TGGAGGTTTCTAGGCAAGCA-3'.

4.3. Infections

Cells were infected using ZIKV (strain MP1751, Uganda), and COXB5 (isolated at Cisanello hospital, Pisa, Italy). A549 cells and NAAA−/− cells were infected with 1 MOI of ZIKV. A549 and A549 NAAA−/− cells were infected with COXB5 at 0.1 MOI. Human NES cells were infected with ZIKV at 0.5 MOI, with or without ARN726 or GW6471 (Merck,

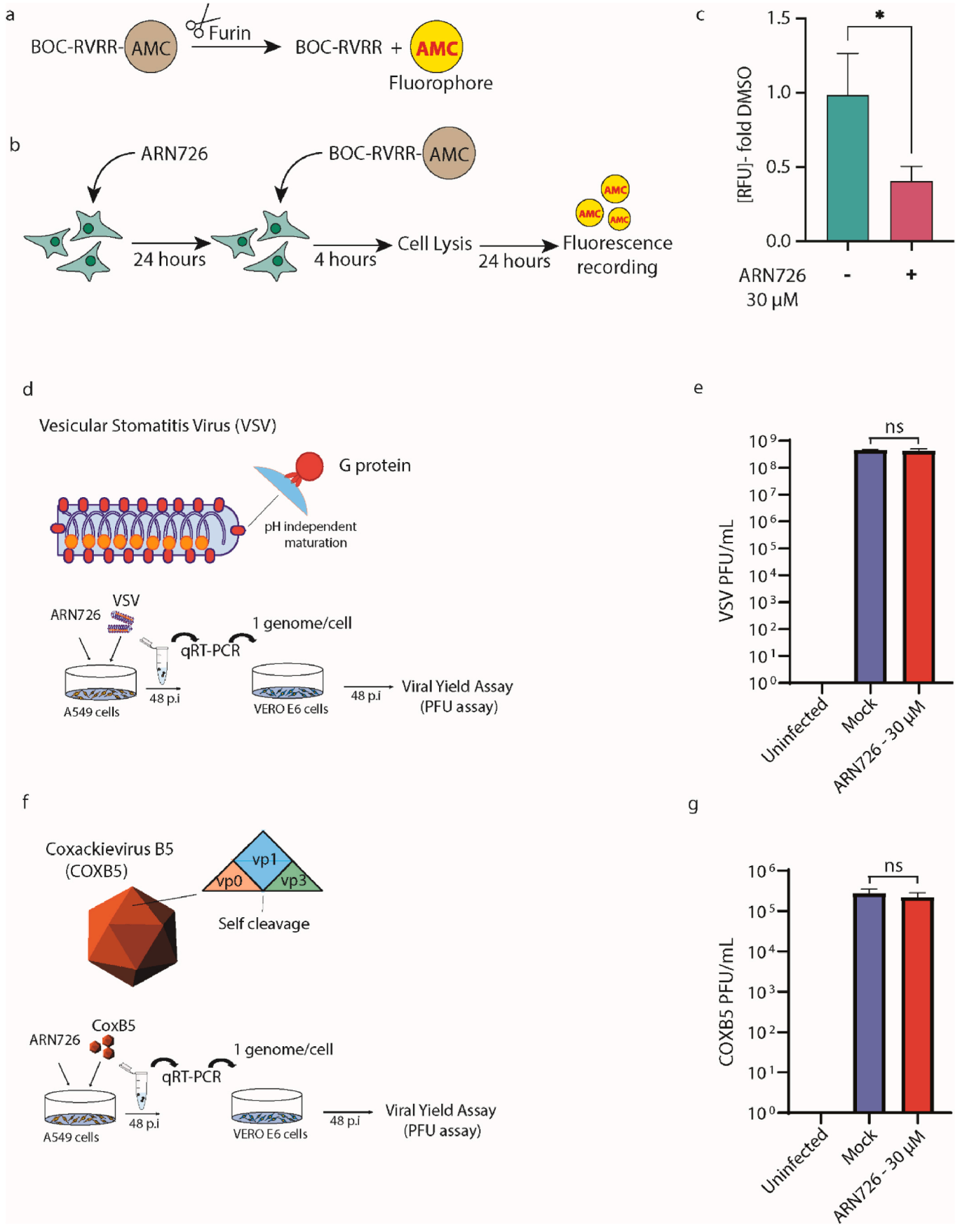

(caption on next page)

Fig. 10. NAAA inhibition does not interfere with VSV and COXB5 infectivity. **a.** Schematic illustration on the mechanism of Furin activity detection. **b.** Schematic illustration of cell-based fluorescence assay to evaluate Furin activity in the presence or not of ARN726. Briefly, cells were pre-treated with ARN726 for 24h, then incubated with the Furin substrate BOC-RVRR-AMC for 4h. Then cells were lysed and analyzed for AMC fluorescence. **c.** Statistical analysis of A549 cells treated or not with ARN726 as described in b. Data are expressed as mean ± SD, N = 3 and analyzed with Student's T test (*p < 0.1; α = 0.5). **d.** Schematic illustration of VSV structure and experimental workflow. A549 cells pretreated or not with ARN726 were infected with VSV 0.1 MOI. 48h p.i, supernatants were quantified for VSV genomes by qRT-PCR and equal quantities of viral genomes were used to infect VERO E6 cells. 48h later, viral yield was quantified by PFU assays. **E.**Vial yield assay performed on VERO cells infected with 1 viral genome/cell of VSV as schematically represented in a. **f.** Schematic illustration of COXB5 structure and experimental workflow as described for VSV in a. **g.** Vial yield assay performed on VERO E6 cells infected with 1 viral genome/cell of COXB5 as schematically represented in c. Data are expressed as mean ± SD, N = 3 and analyzed with Student's T test (ns-not significant.

Darmstadt, Germany) added 15 min before and after infection.

4.4. Western blot analysis

A549 were lysed with RIPA lysis buffer (Millipore, Massachusetts, USA). Membranes were incubated at 4 °C overnight with the following antibodies: anti-NAAA (1:1000, Abnova, Taipei, Taiwan), Anti-ZIKV E (1:1000, Genetex; Irvine, US and anti-β-actin (1:1000, A2066 Sigma-Aldrich, St. Louis, MO 63103, USA). Blots were acquired and analyzed by using Chemidoc XRS system (BioRad, California, USA).

4.5. RNA extraction and qRT-PCR

Total RNA was extracted with QIAzol Lysis Reagent (QIAGEN, Hilden, Germany) according to the manufacturer's instructions. Total RNA (200 ng) was reverse-transcribed in cDNA and amplified by using QuantiNova SYBR Green RT-PCR kit (QIAGEN®, Hilden, Germany). Viral genomes were extracted from the supernatants at different time points post-infection using Takara MiniBEST Viral RNA/DNA (Takara Bio, Kyoto, Japan) according to the manufacturer's instructions. Then RNA was reverse-transcribed and amplified using One Step PrimeScriptTM III RT-qPCR Mix kit (Takara Bio, Kyoto, Japan). Primers and probes: ZIKV: F:5′-TGAGATCAACCACTGCAAGY-3′, R: 5′-GCCTTATCTCCATTCCATACCA -3′, Probe 5′- FAM-ATCGAGGAATGGTGCTGCAGGGA-BHQ1 -3. NAAA: F:5′-AAGACTCCA-GAGGCCACATTTACCATGGTC-3'; R:5′CATCAGCAATAAGGGGAGTCTTGGCCAACT-3. PPAR-α: F: 5′-CTATCATTTGCTGTGGAGATCG-3′, R: 5′-AAGATATCGTCCGGGTGGTT-3′ β-actin: F: 5′AGGAGAAGCTGTGCTACGTC-3′, R: 5′-AGA-CAGCACTGTGTTGGGGTA-3′ hCXCL10: F:5′-CCTGCAAGC-CAATTTTGTCCA-;3′ R: 5′-TGGCATCGATTTTGCTCCCCT-3′ hIL10: F: 5′-CAGGGCACCCAGTCTGAGAAC-3'; R: 5-AGGCTTGGCAACCCAGGTAA-3′ hIL6: F: 5′-CCAGGAGAAGATTCCAAAGATG-3'; R: 5′-GGAAGGTT-CAGGTTGTTTTCTG-3′ hIL8 F:5′CCTGATTTCTGCAGCTCTGTG-3'; R:5′-CCAGACAGAGCTCTCTTCCAT-3'. PGC1-a F: 5′-GAGTCTGTATGGAGT-GACATCG-3′R: 5′-TGTCTGTATCCAAGTCGTTCA-3'.

4.6. Immunostaining and high-content confocal imaging

A549 cells were seeded in 96-CellCarrierUltra plates (PerkinElmer, Hamburg, Germany), then infected or treated as described above. Cells were fixed using 3.7% formaldehyde and stained with the following primary antibodies: anti-NAAA (1:300, Abnova, Taipei, Taiwan), ZIKV: Anti-Flavivirus NS1 antibody (ab214337), nuclei were stained with DAPI (1 μg/mL). Images were acquired using Operetta CLS high-content imaging device (PerkinElmer, Hamburg, Germany) and analyzed with Harmony 4.6 software (PerkinElmer Hamburg, Germany). To investigate the co-localization of ZIKV (C) and NAAA we used the following building blocks: Find Nuclei > Find Cytoplasm > Calculate intensity properties (ZikvC-Alexa 568) > Select population: Infected cells > Find Spot C+ > Find Spot NAAA+ > Calculate position properties (% overlap C+/NAAA+). Similarly, co-localization of ZIKV (C) and Golgi cargoes was performed with the following building blocks: find nuclei > find cytoplasm > Calculate intensity properties (ZIKV C Alexa 568, Golgin-97 Alexa488) > find spots (488+,568+) > calculate position properties (%overlap 488+/568+) ~150 fields were analyzed per well using 63 × water objective, as previously described (Lai et al., 2021b, 2021c).

4.7. ELISA assay

IL-6 and IL-10 were quantified by ELISA assay (Mabtech, Sweden) as manufacturer's instructions. Briefly, samples and standards were incubated for 2hin microwells. Then, wells were washed and incubated with Streptavidin-HRP for 1h. Then, absorbance was recorded at 450 nm.

4.8. Lysosensor blue/yellow

Cells, treated or not with ARN726, were exposed to Lysosensor blue (Thermo Fisher Scientific, 7.5 μM, 5 min, 37 °C), washed to remove any remaining dye, and imaged immediately. For pH quantification, cells were treated with Lysosensor yellow/blue (7.5 μM) after trypsinization and resuspension in Hanks' balanced salt solution containing 20 mM Hepes, 4.5 g/L glucose, and 1% FBS, followed by measurement of fluorescence ratio at 436 and 525 nm (λex 380 nm) after resuspending in Mes buffer, pH 7.0. Boltzmann equation was used to fit the measured ratios to known pH values obtained from calibration curves, and LE/Ly pH was calculated for controls and sample cells. Chloroquine (100 nM; Sigma, St. Louis, MO) was used as a positive control.

4.9. RNA sequencing and analyses

Total RNA was extracted from cells using QIAzol Lysis Reagent according to the manufacturer's instructions (QIAGEN, Hilden, Germany). RNA library was prepared using the QuantSeq 3′ mRNA-Seq Library Prep Kit FWD for Illumina (Lexogen GmbH, Vienna, Austria), following the manufacturer's instructions. Pooled library was then quantified using the Qubit double-stranded DNA (dsDNA) HS Assay Kit on a Qubit 2.0 Fluorometer (Thermo Fisher Scientific, Carlsbad, CA, USA) and diluted to 4 nM following the manufacturer's instructions. The pooled library was denatured and 12 pM were sequenced on MiSeq Illumina platform using the MiSeq Reagent Kit v2 (300 cycles) with a 2 X 150 base pairs (bp) paired-end layout. Trimmed and demultiplexed reads were analyzed using the BlueBee platform (Lexogen GmbH, Vienna, Austria) data analysis workflows for Lexogen RNA-Seq kit in order to obtain the reads count file. Then, differentially expressed genes (DEGs) were determined using R package limma (a Bioconductor package). Differentially expressed genes were defined as genes with a Benjamini–Hochberg multiple-testing adjusted P-value of <0.01. Adjusted P-value was supposed to avoid the occurrence of false-positive results. Genes with the threshold of p-value <0.01 and log2 FoldChange (logFC) ≥ 0.58 between A549 NAAA−/− and WT cells were identified as DEGs. Heatmap2 packages of R were applied to generate heatmap visualization of the most differentially expressed genes as normalized log10 count. The identified DEGs were subjected to Gene Ontology (GO) enrichment analysis. The GO enrichment analysis was carried out by using the R package GOseq. Consequently, based on the above functional enrichment analysis, key genes related to immune response to infections and lipid metabolism were selected to create a bubble plot reporting p-value and the number of DEGs in the biological process category.

4.10. Furin enzyme activity assay

A549 cells were seeded in 96 well black plate and treated with ARN726 30 μM or DMSO, as a control. After 24 h, cells were washed in PBS three times and incubated for 4 h in assay buffer (RPMI, 100 μM furin fluorogenic substrate BOC-RVRR-AMC, 0.1% Triton X-100). The assay buffer was then removed, and cells were washed in PBS. Cells were lysed (Cellytic M, Sigma) for 15 min. After cell lysis, samples were diluted 1:4 in PBS and incubated for additional 24 h at room temperature. Fluorescence was measured using 380 nm for excitation and 460 nm emission recording. The fluorescence data were normalized to cell density and normalized to values obtained with DMSO treated control cells as described by Cortese et al. (2019).

Contributions

M.L conceived and designed the experiments; V.L.R., R.A., E.I., C.F., E.C., A.D.C., D.F, R.F., G.L., P.G.S., M.B., M.O, F.F performed and analyzed the experiments; M.L., G.F., D.P. and M.P. supervised analyses and provided reagents and resources; M.P. provided funding; M.L., G.F., and M.P. wrote the manuscript with input from all other authors.

Declaration of competing interest

The authors declare that they have no known competing financial interests or personal relationships that could have appeared to influence the work reported in this paper.

Data availability

Data will be made available on request.

Acknowledgments

This work was supported by “I-GENE, In-vivo Gene Editing by Nanotransducers”, European call identifier H2020-FETOPEN-2018-2020, Proposal ID 862714. University of Pisa Grant: PRIN 2020 ““DissectINg the complex network of virus-cell Host interactions controlling virAL replication and inflammatory response to identify novel host-targeted approaches against severe respiratory virus infections (INHALA)”. Progetti di Ricerca di Rilevante Interesse Nazionale PRIN 2020, Prot. n. 2020KSY3KL. Progetto di Ricerca di Ateneo 2020, PRA_2020_32 and PRA_2020_37 of the University of Pisa. PNRR - Tuscany Health Ecosystem (THE) – CUP I53C22000780001 – Project code ECS00000017- spoke n. 7 - “Innovating Translational Medicine”. - Subproject 5 - Innovative models for management of infections caused by antibiotic-resistant bacteria. PRIN 2020 “Development of VEGFR/Tubulin and Efflux Pump inhibitors loaded on stimuli-responsive cell membrane coated Nanocarriers for the tratment of Metastatic Cancers” - 20200239N53. We acknowledge CISUP—Centre for Instrumentation Sharing—University of Pisa for the use of Operetta CLS imaging facility and Mass Spectrometry facility.

Appendix A. Supplementary data

Supplementary data to this article can be found online at https://doi.org/10.1016/j.antiviral.2023.105664.

References

Adler, D.H., Cogan, J.D., Phillips, J.A., Schnetz-Boutaud, N., Milne, G.L., Iverson, T., Stein, J.A., Brenner, D.A., Morrow, J.D., Boutaud, O., Oates, J.A., 2008. Inherited human cPLA(2alpha) deficiency is associated with impaired eicosanoid biosynthesis, small intestinal ulceration, and platelet dysfunction. J. Clin. Invest. 118, 2121–2131.

Basavappa, R., Syed, R., Flore, O., Icenogle, J.P., Filman, D.J., Hogle, J.M., 1994. Role and mechanism of the maturation cleavage of VP0 in poliovirus assembly: structure of the empty capsid assembly intermediate at 2.9 A resolution. Protein Sci. 3, 1651–1669.

Bougarne, N., Weyers, B., Desmet, S.J., Deckers, J., Ray, D.W., Staels, B., De Bosscher, K., 2018. Molecular actions of PPARα in lipid metabolism and inflammation. Endocr. Rev. 39, 760–802.

Butler, D., 2016. Brazil asks whether Zika acts alone to cause birth defects. Nature 535, 475–476.

Caldas, L.A., Azevedo, R.C., da Silva, J.L., de Souza, W., 2020. Microscopy analysis of Zika virus morphogenesis in mammalian cells. Sci. Rep. 10, 8370.

Calder, P.C., 2020. -3 PUFA and inflammation: from membrane to nucleus and from bench to bedside. Proc. Nutr. Soc. 1–13.

Čaval, T., Zhu, J., Tian, W., Remmelzwaal, S., Yang, Z., Clausen, H., Heck, A.J.R., 2019. Targeted analysis of lysosomal directed proteins and their sites of mannose-6-phosphate modification. Mol. Cell. Proteomics 18, 16–27.

Cortese, M., Kumar, A., Matula, P., Kaderali, L., Scaturro, P., Erfle, H., Acosta, E.G., Buehler, S., Ruggieri, A., Chatel-Chaix, L., Rohr, K., Bartenschlager, R., 2019. Reciprocal effects of fibroblast growth factor receptor signaling on dengue virus replication and virion production. Cell Rep. 27, 2579–2592.e6.

Da Poian, A.T., Carneiro, F.A., Stauffer, F., 2005. Viral membrane fusion: is glycoprotein G of rhabdoviruses a representative of a new class of viral fusion proteins? Braz. J. Med. Biol. Res. 38, 813–823.

De Filippis, D., Negro, L., Vaia, M., Cinelli, M.P., Iuvone, T., 2013. New insights in mast cell modulation by palmitoylethanolamide. CNS Neurol. Disord.: Drug Targets 12, 78–83.

de Silva, A.M., Rey, F.A., Young, P.R., Hilgenfeld, R., Vasudevan, S.G., 2018. Viral entry and NS1 as potential antiviral drug targets. Adv. Exp. Med. Biol. 1062, 107–113.

Di Stadio, A., D'Ascanio, L., Vaira, L.A., Cantone, E., De Luca, P., Cingolani, C., Motta, G., De Riu, G., Vitelli, F., Spriano, G., De Vincentiis, M., Camaioni, A., La Mantia, I., Ferreli, F., Brenner, M.J., 2022. Ultramicronized palmitoylethanolamide and luteolin supplement combined with olfactory training to treat post-COVID-19 olfactory impairment: a multi-center double-blinded randomized placebo- controlled clinical trial. Curr. Neuropharmacol. 20, 2001–2012.

Dias, S.S.G., Soares, V.C., Ferreira, A.C., Sacramento, C.Q., Fintelman-Rodrigues, N., Temerozo, J.R., Teixeira, L., Nunes da Silva, M.A., Barreto, E., Mattos, M., de Freitas, C.S., Azevedo-Quintanilha, I.G., Manso, P.P.A., Miranda, M.D., Siqueira, M. M., Hottz, E.D., Pão, C.R.R., Bou-Habib, D.C., Barreto-Vieira, D.F., Bozza, F.A., Souza, T.M.L., Bozza, P.T., 2020. Lipid droplets fuel SARS-CoV-2 replication and production of inflammatory mediators. PLoS Pathog. 16, e1009127.

Gorelik, A., Gebai, A., Illes, K., Piomelli, D., Nagar, B., 2018. Molecular mechanism of activation of the immunoregulatory amidase NAAA. Proc. Natl. Acad. Sci. U. S. A. 115, E10032-E10040.

Hammock, B.D., Wang, W., Gilligan, M.M., Panigrahy, D., 2020. Eicosanoids: the overlooked storm in coronavirus disease 2019 (COVID-19)? Am. J. Pathol. 190, 1782–1788.

Heymann, D.L., Hodgson, A., Sall, A.A., Freedman, D.O., Staples, J.E., Althabe, F., Baruah, K., Mahmud, G., Kandun, N., Vasconcelos, P.F., Bino, S., Menon, K.U., 2016. Zika virus and microcephaly: why is this situation a PHEIC? Lancet 387, 719–721.

Kam, Y.W., Leite, J.A., Lum, F.M., Tan, J.J.L., Lee, B., Judice, C.C., Teixeira, D.A.T., Andreata-Santos, R., Vinolo, M.A., Angerami, R., Resende, M.R., Freitas, A.R.R., Amaral, E., Junior, R.P., Costa, M.L., Guida, J.P., Arns, C.W., Ferreira, L.C.S., Rénia, L., Proença-Modena, J.L., Ng, L.F.P., Costa, F.T.M., Network, Z.-U., 2017. Specific biomarkers associated with neurological complications and congenital central nervous system abnormalities from Zika virus-infected patients in Brazil. J. Infect. Dis. 216, 172–181.

Keppel Hesselink, J.M., de Boer, T., Witkamp, R.F., 2013. Palmitoylethanolamide: a natural body-own anti-inflammatory agent, effective and safe against influenza and common cold. Int. J. Inflamm., 151028, 2013.

Lai, M., Iacono, E., Spezia, P.G., Lottini, G., La Rocca, V., Quaranta, P., Pistello, M., Freer, G., 2021a. A low-cost simple test for weekly detection of Mycoplasma hyorhinis and arginini contaminations in cell cultures and viral preparations. J. Virol Methods 299, 114327.

Lai, M., La Rocca, V., Amato, R., Freer, G., Costa, M., Spezia, P.G., Quaranta, P., Lombardo, G., Piomelli, D., Pistello, M., 2021b. Ablation of acid ceramidase impairs autophagy and mitochondria activity in melanoma cells. Int. J. Mol. Sci. 22.

Lai, M., Amato, R., La Rocca, V., Bilgin, M., Freer, G., Spezia, P., Quaranta, P., Piomelli, D., Pistello, M., 2021c. Acid ceramidase controls apoptosis and increases autophagy in human melanoma cells treated with doxorubicin. Sci. Rep. 11, 11221.

Lai, M., Maori, E., Quaranta, P., Matteoli, G., Maggi, F., Sgarbanti, M., Crucitta, S., Pacini, S., Turriziani, O., Antonelli, G., Heeney, J.L., Freer, G., Pistello, M., 2021d. CRISPR/Cas9 ablation of integrated HIV-1 accumulates proviral DNA circles with reformed long terminal repeats. J. Virol. 95, e0135821.

Lai, M., De Carli, A., Filipponi, C., Iacono, E., La Rocca, V., Lottini, G., Piazza, C.R., Quaranta, P., Sidoti, M., Pistello, M., Freer, G., 2022. Lipid balance remodelling by human positive-strand RNA viruses and the contribution of lysosomes. Antivir. Res. 206, 105398.

Lottini, G., Baggiani, M., Chesi, G., D'Orsi, B., Quaranta, P., Lai, M., Pancrazi, L., Onorati, M., Pistello, M., Freer, G., Costa, M., 2022. Zika virus induces FOXG1 nuclear displacement and downregulation in human neural progenitors. Stem Cell Rep. 17, 1683–1698.

Luu, A.P., Yao, Z., Ramachandran, S., Azzopardi, S.A., Miles, L.A., Schneider, W.M., Hoffmann, H.H., Bozzacco, L., Garcia, G., Gong, D., Damoiseaux, R., Tang, H., Morizono, K., Rudin, C.M., Sun, R., Arumugaswami, V., Poirier, J.T., MacDonald, M. R., Rice, C.M., Li, M.M.H., 2021. A CRISPR activation screen identifies an atypical rho GTPase that enhances Zika viral entry. Viruses 13.

Martín-Acebes, M.A., Vázquez-Calvo, Á., Saiz, J.C., 2016. Lipids and flaviviruses, present and future perspectives for the control of dengue, Zika, and West Nile viruses. Prog. Lipid Res. 64, 123–137.
Merad, M., Martin, J.C., 2020. Pathological inflammation in patients with COVID-19: a key role for monocytes and macrophages. Nat. Rev. Immunol. 20, 355–362.
Migliore, M., Pontis, S., Fuentes de Arriba, A.L., Realini, N., Torrente, E., Armirotti, A., Romeo, E., Di Martino, S., Russo, D., Pizzirani, D., Summa, M., Lanfranco, M., Ottonello, G., Busquet, P., Jung, K.M., Garcia-Guzman, M., Heim, R., Scarpelli, R., Piomelli, D., 2016. Second-generation non-covalent NAAA inhibitors are protective in a model of multiple sclerosis. Angew Chem. Int. Ed. Engl. 55, 11193–11197.
Molloy, S.S., Thomas, L., VanSlyke, J.K., Stenberg, P.E., Thomas, G., 1994. Intracellular trafficking and activation of the furin proprotein convertase: localization to the TGN and recycling from the cell surface. EMBO J. 13, 18–33.
Mottillo, E.P., Bloch, A.E., Leff, T., Granneman, J.G., 2012. Lipolytic products activate peroxisome proliferator-activated receptor (PPAR) α and δ in brown adipocytes to match fatty acid oxidation with supply. J. Biol. Chem. 287, 25038–25048.
Ornelas, A.M., Pezzuto, P., Silveira, P.P., Melo, F.O., Ferreira, T.A., Oliveira-Szejnfeld, P. S., Leal, J.I., Amorim, M.M., Hamilton, S., Rawlinson, W.D., Cardoso, C.C., Nixon, D. F., Tanuri, A., Melo, A.S., Aguiar, R.S., 2017. Immune activation in amniotic fluid from Zika virus-associated microcephaly. Ann. Neurol. 81, 152–156.
Piomelli, D., Scalvini, L., Fotio, Y., Lodola, A., Spadoni, G., Tarzia, G., Mor, M., 2020. -Acylethanolamine acid amidase (NAAA): structure, function, and inhibition. J. Med. Chem. 63, 7475–7490.
Sasso, O., Moreno-Sanz, G., Martucci, C., Realini, N., Dionisi, M., Mengatto, L., Duranti, A., Tarozzo, G., Tarzia, G., Mor, M., Bertorelli, R., Reggiani, A., Piomelli, D., 2013. Antinociceptive effects of the N-acylethanolamine acid amidase inhibitor ARN077 in rodent pain models. Pain 154, 350–360.
Sirohi, D., Kuhn, R.J., 2017. Zika virus structure, maturation, and receptors. J. Infect. Dis. 216, S935–S944.
Stadler, K., Allison, S.L., Schalich, J., Heinz, F.X., 1997. Proteolytic activation of tick-borne encephalitis virus by furin. J. Virol. 71, 8475–8481.
Taylor, B.K., 2013. N-acylethanolamine acid amidase (NAAA), a new path to unleash PPAR-mediated analgesia. Pain 154, 326–327.
Vaney, M.C., Dellarole, M., Duquerroy, S., Medits, I., Tsouchnikas, G., Rouvinski, A., England, P., Stiasny, K., Heinz, F.X., Rey, F.A., 2022. Evolution and activation mechanism of the flavivirus class II membrane-fusion machinery. Nat. Commun. 13, 3718.
Wang, Z., Li, S., Huang, B., 2022. Alveolar macrophages: achilles' heel of SARS-CoV-2 infection. Signal Transduct. Targeted Ther. 7, 242.
Wu, K., Xiu, Y., Zhou, P., Qiu, Y., Li, Y., 2019. A new use for an old drug: carmofur attenuates lipopolysaccharide (LPS)-Induced acute lung injury. Front. Pharmacol. 10, 818.
Yoneyama, M., Fujita, T., 2009. RNA recognition and signal transduction by RIG-I-like receptors. Immunol. Rev. 227, 54–65.
Yu, S., Rao, S., Reddy, J.K., 2003. Peroxisome proliferator-activated receptors, fatty acid oxidation, steatohepatitis and hepatocarcinogenesis. Curr. Mol. Med. 3, 561–572.
Yu, I.M., Zhang, W., Holdaway, H.A., Li, L., Kostyuchenko, V.A., Chipman, P.R., Kuhn, R. J., Rossmann, M.G., Chen, J., 2008. Structure of the immature dengue virus at low pH primes proteolytic maturation. Science 319, 1834–1837.
Yu, I.M., Holdaway, H.A., Chipman, P.R., Kuhn, R.J., Rossmann, M.G., Chen, J., 2009. Association of the pr peptides with dengue virus at acidic pH blocks membrane fusion. J. Virol. 83, 12101–12107.
Zhang, F., Hammack, C., Ogden, S.C., Cheng, Y., Lee, E.M., Wen, Z., Qian, X., Nguyen, H. N., Li, Y., Yao, B., Xu, M., Xu, T., Chen, L., Wang, Z., Feng, H., Huang, W.K., Yoon, K. J., Shan, C., Huang, L., Qin, Z., Christian, K.M., Shi, P.Y., Xia, M., Zheng, W., Wu, H., Song, H., Tang, H., Ming, G.L., Jin, P., 2016. Molecular signatures associated with ZIKV exposure in human cortical neural progenitors. Nucleic Acids Res. 44, 8610–8620.